Voltage/Current Doubler Converter for an Efficient Wireless Charging of Electric Vehicles With 400V and 800V Battery Voltages

Grazian, Francesca; Soeiro, Thiago Batista; Bauer, Pavol

DOI
10.1109/TIE.2022.3208582

Publication date
2023

Document Version
Final published version

Published in
IEEE Transactions on Industrial Electronics

Voltage/Current Doubler Converter for an Efficient Wireless Charging of Electric Vehicles With 400-V and 800-V Battery Voltages

Francesca Grazian, *Student Member, IEEE*, Thiago Batista Soeiro, *Senior Member, IEEE*, and Pavol Bauer, *Senior Member, IEEE*

***Abstract*—The lithium-ion battery of an electric vehicle (EV) is typically rated at either 400 or 800 V. When considering public parking infrastructures, EV wireless chargers must efficiently deliver electric power to both battery options. This can be normally achieved by regulating the output voltage through a dc–dc converter at the cost of higher onboard circuit complexity and lower overall efficiency. This article proposes a wireless charging system that maintains a high power transfer efficiency when charging EVs with either 400- or 800-V nominal battery voltage at the same power level. The control scheme is implemented at the power source side, and only passive semiconductor devices are employed on board the EV. The presented system, called voltage/current doubler (V/I-D), comprises two sets of series-compensated coupled coils, each of them connected to a dedicated H-bridge converter. The equivalent circuit has been analyzed while explaining the parameters' selection. The analytical power transfer efficiency has been compared to the one resulting from the conventional one-to-one coil system at 7.2 kW. For the same power level, the dc-to-dc efficiency of 97.11% and 97.52% have been measured at 400-V and 800-V voltage output, respectively. Finally, the functionality of the V/I-D converter has been proved at both the even and uneven misalignments of the two sets of coupled coils.**

***Index Terms*—Battery voltage, electric vehicles (EVs), inductive power transfer, wireless charging.**

I. Introduction

INDUCTIVE power transfer (IPT) employed for battery wireless charging has been gaining interest in the electric vehicle (EV) industry mainly because it would solve the drivers' inconvenience in handling charging cables.

As more EV models crowd the streets, it is noticeable that their nominal battery voltage is not necessarily the same. According to [1], the nominal voltage of EV batteries could mostly be either 400 or 800 V, which is confirmed by Table I. The first released EVs have a nominal battery voltage of around 400 V since more automotive-qualified components are available for that voltage class. However, some automotive original-equipment manufacturers are moving to 800-V architectures because the higher dc-link voltage results in two main advantages, being the substantial weight saving across the EV and the considerable reduction of the battery charging time [2], [3], [4]. Especially when considering applications such as public parking infrastructures, taxi pick-up locations in front of stations or airports, corporate fleets, car rental, or sharing facilities, it is essential that wireless chargers can supply power efficiently to both the EV battery classes.

TABLE I
List of Commercial EVs and Their Battery Voltage

Year of launch	Manufacturer	Model	Battery voltage (latest model)	Source
2018	Audi	e-tron	396 V	[8], [9]
2020	FIAT	new 500e	364 V	[8]
2019	Mercedes-Benz	EQC	405 V	[8]
2021		EQA	420 V	
2022		EQB	420 V	
2013	Nissan	Leaf S	350 V	[8]
2010		Leaf SV Leaf SL	360 V	[8], [10]
2012	Tesla	Model S	400 V	[8], [11]
		Model X	350 V	[8]
2017		Model 3	360 V	
2010	Volkswagen	e-up!	374 V	[8]
2014		e-Golf	323 V	[8], [12]
2019		ID.3	408 V	[8]
2019	Aston Martin	Rapide E	800 V	[8]
2021	Hyundai	IONIQ 5	800 V	[8], [13]
2021	KIA	EV6	697 V	[8]
2019	Porsche	Taycan	800 V	[8], [14]

IPT systems with magnetic resonance coupling are intrinsically isolated resonant converters with a loosely coupled transformer. As previously demonstrated in [5], [6], and [7], these systems can achieve high power transfer efficiency when operating at the nominal operating condition for a certain power level, i.e., at the chosen converter's voltage gain defined as the ratio between the input and output voltages. Charging a battery with either double or half of the nominal voltage would dramatically worsen the system efficiency for the same output power. In IPT systems, this can be explained because, in those conditions, the equivalent operating resistive load would differ four times

Manuscript received 13 May 2022; revised 9 August 2022; accepted 10 September 2022. Date of publication 28 September 2022; date of current version 15 March 2023. *(Corresponding author: Francesca Grazian.)*

The authors are with the Department of Electrical Sustainable Energy, Delft University of Technology, 2628 CD Delft, The Netherlands (e-mail: f.grazian@tudelft.nl; tbsoeiro@gmail.com; p.bauer@tudelft.nl).

Color versions of one or more figures in this article are available at https://doi.org/10.1109/TIE.2022.3208582.

Digital Object Identifier 10.1109/TIE.2022.3208582

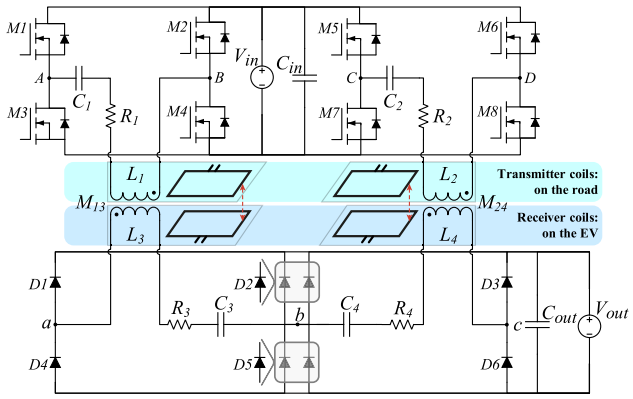

Fig. 1. Circuit of the V/I-D converter for battery charging applications through IPT. Herein, $D2$ and $D5$ can be advantageously assembled with two parallel diodes of the same technology used in $D1$, $D3$, $D4$, and $D6$. In this case, for a given charging power independently of the operation, the current rating of the converter's circuit components is similar.

from the equivalent optimum load defined in [15] and [16]. At the current date, no research has been found in the available literature on EV wireless charging systems that can efficiently provide both the 400- and 800-V batteries with the same power.

The efficiency degradation that occurs when the battery voltage differs from the nominal could be mitigated in several ways. One solution could be charging 400- and 800-V batteries at different power levels to match the optimum load condition. This would result in delivering one-fourth of the nominal power to 400-V batteries. However, when considering the wireless charging of light-duty EVs, SAE J2954 defines three power classes for wireless chargers. These power classes limit the maximum input power obtainable from the grid connection to 3.7, 7.7, and 11.1 kVA. Charging 400-V batteries with lower power than 800-V batteries means that the power capability of a wireless charging transmitter belonging to a specific SAE J2954 power class would not be fully utilized. Consequently, this would extend considerably the charging times, which might already be quite long at these power levels. Therefore, it is preferable to fully utilize the power available from the grid connection when charging both 400- and 800-V batteries. Alternatively, a dc–dc converter can be employed between the IPT system's output and the EV battery. In this way, the IPT system would still operate at the nominal voltage gain, while the dc–dc converter sets the required voltage ratio and power exchange. In other words, the equivalent operating load would still match the optimum load condition, and consequently, the worsening of the power transfer efficiency of the IPT system would only depend on the performance of the dc–dc converter. Nevertheless, using a dc–dc converter would increase the complexity of the circuit and the control onboard the EV, which is not preferable.

This article proposes an IPT system that can charge both the 400- and 800-V EV battery classes at the same output power while maintaining high power transfer efficiency. This guarantees that the available power from the grid connection is fully utilized. The proposed circuit takes the name of voltage/current doubler (V/I-D), and it is illustrated in Fig. 1. This consists of two H-bridge inverters, two sets of coupled coils with their series-series (S-S) compensation, and two full-wave diode rectifiers. The control is only implemented at the power source circuit resulting in an onboard circuit with only passive devices. It must be noted that the V/I-D converter is a universal solution for both the EV battery classes, which makes its installation practical and it eases its later reconfiguration.

The rest of this article is organized as follows. The analytical modeling, equivalent circuit, and operation of the V/I-D converter are discussed in Section II. In Section III, the comparison with the standard one-to-one coil IPT system is performed. The laboratory demonstrator of the V/I-D converter and the expected operating points are discussed in Section IV. The proposed concept is proved experimentally in Section V at the power level of 7.7 kW with aligned and misaligned coils. Finally, Section VI concludes this article.

II. V/I-D Converter

The V/I-D converter in Fig. 1 delivers the same output power to 400- and 800-V batteries depending on the modulation of the two H-bridge inverters. A similar strategy has been used in [17] and [18] to achieve a wide output voltage regulation. For that purpose, Zhang and Zhang [17] propose a phase-shifted multiple H-bridge dc–dc power supply (nonresonant), while Wu et al. [18] use an interleaved *LLC* resonant converter with variable frequency and phase shift. However, these topologies fundamentally differ from the proposed V/I-D converter because they use highly coupled transformers. Thereby, the output voltage is regulated by continuously controlling the phase-shift angle between the two H-bridge inverters in the range 0–180°. This cannot be applied directly to IPT systems for battery charging since the output voltage is given by the battery. Moreover, controlling that phase-shift angle in the entire range is not suitable for IPT systems since it would lead to an unbalance of the two input impedances, resulting in the hard switching of one of the H-bridge inverters, while the other would be operating deeply in the inductive region. Thus, the proposed V/I-D converter in Fig. 1 is an original concept for IPT systems for battery charging.

A. Circuit Analysis and Operation

When the half-bridge legs with midpoints A and C have the modulation shown in Fig. 2(a), the current through the secondary coils has the same direction, and consequently, L_3 and L_4 result in a series connection. In the rectification stage, only $D1$ and $D6$ conduct during the positive half-wave of V_{ac}, while $D3$ and $D4$ conduct in the negative one. The two secondary coils conduct the same nominal current as shown in Fig. 3(a). This modulation is called voltage doubler mode since it is suitable for the rated power charging of 800-V batteries.

Contrarily, when the half-bridge legs with midpoints A and D have the modulation shown in Fig. 2(b), the current through the secondary coils has opposite direction, and consequently, L_3 and L_4 result in an equivalent parallel connection. In this case, $D1$, $D3$, and $D5$ conduct during the positive half-wave of V_{ab}, while $D2$, $D4$, and $D6$ conduct during the negative one. Fig. 3 shows

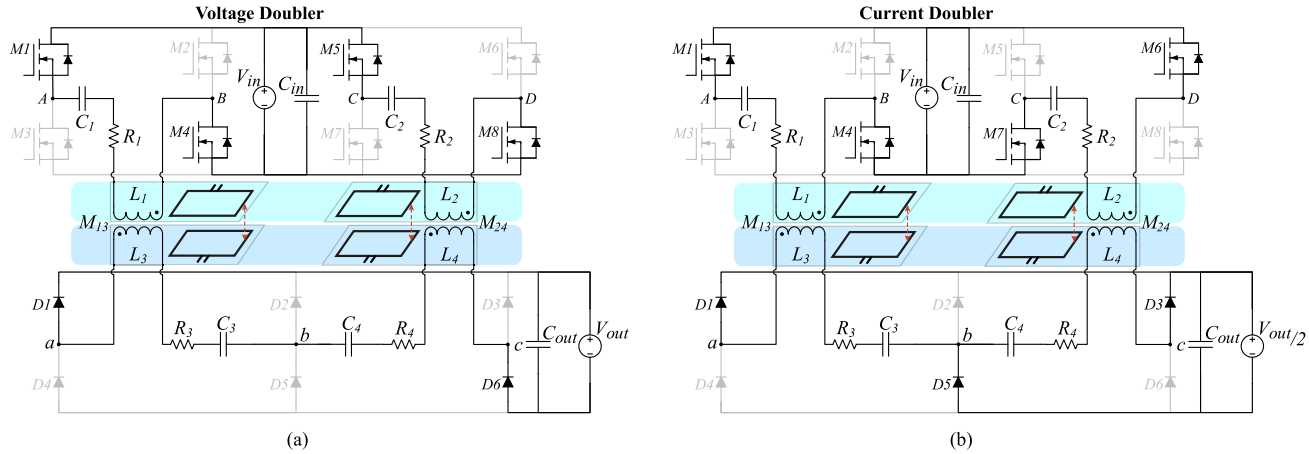

Fig. 2. Semiconductor devices conducting during the positive half wave of $\boldsymbol{V}_{AB}$ when the V/I-D converter operates as: (a) voltage doubler and (b) current doubler, which typical operating waveforms and equivalent circuits are shown in Figs. 3(a) and 4(a), and Figs. 3(b) and 4(b), respectively.

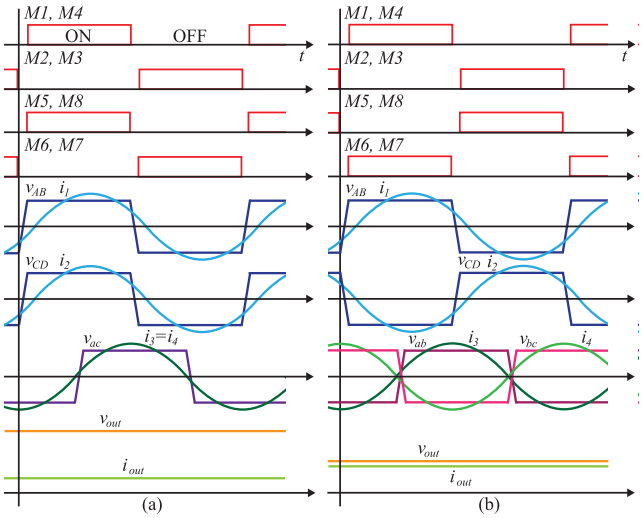

Fig. 3. Typical waveforms of the V/I-D converter operating as: (a) voltage doubler and (b) current doubler, resulting from the operation in Fig. 2.

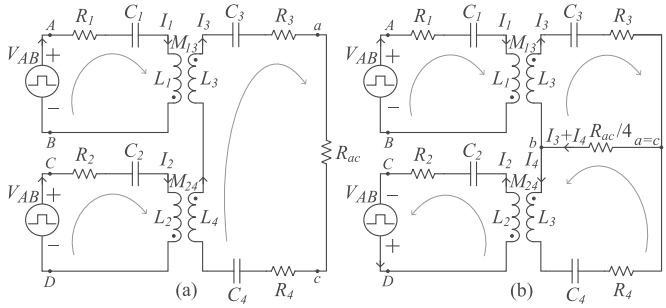

Fig. 4. Equivalent circuit in the frequency domain of Fig. 1 when operating as (a) voltage doubler and (b) current doubler.

that the secondary coils conduct the same nominal current as in the previous modulation, but their parallel connection results in double the load current. This modulation is called current doubler mode since it is suitable for the rated power charging of 400-V batteries.

The equivalent circuit in the frequency domain of the voltage doubler mode is shown in Fig. 4(a), while the one of the current doubler mode is shown in Fig. 4(b). The circuit in Fig. 4(a) is described by the Kirchhoff voltage law in (1) shown at the bottom of this page, while the one in Fig. 4(b) is described by (2) shown at the bottom of this page. Thereby, the EV battery is replaced by the equivalent first-harmonic load R_{ac} in (3) defined

$$\begin{bmatrix} \boldsymbol{V_{AB}} \\ \boldsymbol{V_{CD}} \\ 0 \\ 0 \end{bmatrix} = \begin{bmatrix} \boldsymbol{Z_1} & j\omega M_{12} & j\omega(M_{13}+M_{14}) & 0 \\ j\omega M_{12} & \boldsymbol{Z_2} & j\omega(M_{23}+M_{24}) & 0 \\ j\omega(M_{13}+M_{14}) & j\omega(M_{23}+M_{24}) & (\boldsymbol{Z_3}+\boldsymbol{Z_4}+R_{\text{ac}}+2j\omega M_{34}) & 0 \\ 0 & 0 & 1 & -1 \end{bmatrix} \begin{bmatrix} \boldsymbol{I_1} \\ \boldsymbol{I_2} \\ \boldsymbol{I_3} \\ \boldsymbol{I_4} \end{bmatrix} \tag{1}$$

$$\begin{bmatrix} \boldsymbol{V_{AB}} \\ \boldsymbol{V_{CD}} \\ 0 \\ 0 \end{bmatrix} = \begin{bmatrix} \boldsymbol{Z_1} & -j\omega M_{12} & j\omega M_{13} & -j\omega M_{14} \\ -j\omega M_{12} & \boldsymbol{Z_2} & -j\omega M_{23} & j\omega M_{24} \\ j\omega M_{13} & -j\omega M_{23} & \left(\boldsymbol{Z_3}+\dfrac{R_{\text{ac}}}{4}\right) & \left(-j\omega M_{34}+\dfrac{R_{\text{ac}}}{4}\right) \\ -j\omega M_{14} & j\omega M_{24} & \left(-j\omega M_{34}+\dfrac{R_{\text{ac}}}{4}\right) & \left(\boldsymbol{Z_4}+\dfrac{R_{\text{ac}}}{4}\right) \end{bmatrix} \begin{bmatrix} \boldsymbol{I_1} \\ \boldsymbol{I_2} \\ \boldsymbol{I_3} \\ \boldsymbol{I_4} \end{bmatrix} \tag{2}$$

in [19] and [20]

$$R_{\text{ac}} = \frac{8}{\pi^2} R_L = \frac{8}{\pi^2} \frac{V_{\text{out,max}}^2}{P_{\text{out}}}. \tag{3}$$

Thereby, the impedance $\boldsymbol{Z_i}$ of each resonant circuit is defined in (4), and the mutual inductances M_{ih} are expressed in (5), which depend on the coupling factor k_{ih}. Figs. 1, 2, and 4 highlight only M_{13} and M_{24} since they are the main mutual inductances functional to the operation of the V/I-D converter. On the other hand, M_{12} and M_{34} are due to the cross-coupling present between the two coils placed at each side of the two transformers, while M_{14} and M_{23} are due to the diagonal cross-coupling between the two transformers. $\boldsymbol{V_{AB}}$ is taken as reference according to the phasor convention, and it is defined in (6) through the first-harmonic approximation

$$\boldsymbol{Z_i} = R_i + j\omega X_i, \quad X_i = \omega L_i - \frac{1}{\omega C_i}, \quad i = 1, \ldots, 4 \tag{4}$$

$$M_{ih} = M_{hi} = k_{ih}\sqrt{L_i L_h}, \quad i, h = 1, \ldots, 4 \wedge i \neq h \tag{5}$$

$$\boldsymbol{V_{AB}} = V_{AB}\angle 0^\circ = \frac{4}{\pi} V_{\text{in}}, \quad V_{AB} = V_{CD}. \tag{6}$$

In addition, for a given processed power, the V/I-D resonant circuit's efficiency η_{res} is defined as

$$\eta_{\text{res}} = \begin{cases} \dfrac{R_{\text{ac}}|\boldsymbol{I_3}|^2}{V_{AB}(|\operatorname{Re}[\boldsymbol{I_1}]| + |\operatorname{Re}[\boldsymbol{I_2}]|)}, & \text{if voltage doubler [from (1)]} \\ \dfrac{\frac{R_{\text{ac}}}{4}(|\boldsymbol{I_3}| + |\boldsymbol{I_4}|)^2}{V_{AB}(|\operatorname{Re}[\boldsymbol{I_1}]| + |\operatorname{Re}[\boldsymbol{I_2}]|)}, & \text{if current doubler [from (2)]} \end{cases}. \tag{7}$$

The total dc-to-dc efficiency $\eta_{\text{DC-to-DC}}$ also considers the power losses of the inverting and rectifying stages of which parameters can be extrapolated from the devices' datasheet.

The power losses of the H-bridge inverters are

$$P_{\text{inv}} = 4 \cdot R_{\text{ds,on}} \cdot \left[\left(\frac{\hat{I}_1}{2} \right)^2 + \left(\frac{\hat{I}_2}{2} \right)^2 \right] + E_{\text{sw}} \cdot f_0 \tag{8}$$

where $R_{\text{ds,on}}$ is the ON-resistance of the MOSFETs and E_{sw} is the total switching energy loss defined in (9). Thereby, E_{off} is the turn-OFF energy loss, E_{on} is the turn-ON energy loss, and Q_{rr} is the reverse recovery charge of the body diode

$$E_{\text{sw}} = \sum_{i=1}^{8} E_{\text{off}_{(Mi)}} + \sum_{i=1}^{8} E_{\text{on}_{(Mi)}} + \sum_{i=1}^{8} Q_{\text{rr}_{(Mi)}} V_{\text{ds,off}}. \tag{9}$$

Since C_3 and C_4 are chosen such that $X_3 \approx X_4 \approx 0$, the rectifier's power losses are mainly due to the conduction

$$P_{\text{rect}} = \begin{cases} 4 \cdot \left[V_F \left(\dfrac{\hat{I}_3}{\pi} \right) + r \left(\dfrac{\hat{I}_3}{2} \right)^2 \right], & \text{if V-Doubler} \\ 4 \cdot \left[V_F \left(\dfrac{\hat{I}_3 + \hat{I}_4}{\pi} \right) + r \left(\dfrac{\hat{I}_3 + \hat{I}_4}{2} \right)^2 \right], & \text{if I-Doubler} \end{cases}. \tag{10}$$

In (10), it is assumed that diodes $D2$ and $D5$ are assembled with two parallel diodes of the same technology used in $D1$, $D3$, $D4$, and $D6$. Therein, V_F is the constant voltage (CV) drop of the bipolar technology, while r models the linear increment of the voltage drop across the diode as a function of the flowing current.

Finally, $\eta_{\text{DC-to-DC}}$ can be computed as

$$\eta_{\text{DC-to-DC}} = \eta_{\text{res}} \cdot \frac{P_{\text{out}}}{P_{\text{out}} + P_{\text{inv}} + P_{\text{rec}}}. \tag{11}$$

B. Selection of Circuit Parameters

The parameters of the V/I-D converter must be chosen to ensure high power transfer efficiency. For simplicity, the parameter selection criteria consider the symmetry in (12) between the primary and secondary circuits. In addition, Section V will prove the functionality of the V/I-D converter even in the case that this ideal symmetry is not met

$$\begin{aligned} L_1 = L_2 = L_{1D}, \quad L_3 = L_4 = L_{2D} \\ R_1 = R_2 = R_{1D}, \quad R_3 = R_4 = R_{2D} \\ M_D = M_{13} = M_{24}, \quad k_D = k_{13} = k_{24}. \end{aligned} \tag{12}$$

In (12), L_{1D} and R_{1D} are the self-inductance and the resistance of the primary coils, respectively, L_{2D} and R_{2D} are the self-inductance and the resistance of the secondary coils, respectively, M_D is the value of both main functional mutual inductances, and k_D is their relative coupling factor. Moreover, it is assumed that the coils' cross-coupling is negligible.

The choice of L_{1D} and L_{2D} follows from (14) to (16). The first condition in (14) ensures that the conduction losses in the primary and secondary circuits are balanced. To achieve that, the ratio between the coils' resistances R_{1D} and R_{2D} must be dependent on the ratio between the maximum dc input voltage $V_{\text{in,max}}$ available and the minimum battery voltage $V_{\text{out,min}}$, which has been derived from (13). The second condition in (15) has been found by assuming that the coils' quality factors Q_{1D} and Q_{2D} differ from the constant a, which depends on the coils' geometry and structure. Finally, the target value of mutual inductance M_D can be found from (16), which is well known from the S-S compensation. M_D depends on $V_{\text{in,max}}$, the maximum battery voltage $V_{\text{out,max}}$, the target output power P_{out}, and the resonant angular frequency $\omega_0 = 2\pi f_0$. Finally, the values of L_{1D} and L_{2D} resulting from (14) to (16) are shown in (17)

$$\hat{I}_{1D} = \frac{\pi}{2} I_{\text{in}}, \quad \hat{I}_{2D} = \frac{\pi}{2} I_{\text{out}}$$

$$P_{\text{in}} \approx P_{\text{out}} \quad \rightarrow \quad \frac{I_{\text{in}}}{I_{\text{out}}} = \frac{V_{\text{out,min}}}{V_{\text{in,max}}} = \frac{I_{1D}}{I_{2D}} \tag{13}$$

$$\begin{cases} R_{1D} I_{1D}^2 = R_{2D} I_{2D}^2 \quad \rightarrow \quad \dfrac{R_{1D}}{R_{2D}} = \dfrac{I_{2D}^2}{I_{1D}^2} = \dfrac{V_{\text{in,max}}^2}{V_{\text{out,min}}^2} & (14) \\ Q_{1D} = a \cdot Q_{2D} \quad \rightarrow \quad \dfrac{\omega_0 L_{1D}}{R_{1D}} = \dfrac{a \cdot \omega_0 L_{2D}}{R_{2D}} & (15) \\ M_D = \dfrac{8}{\pi^2} \dfrac{V_{\text{in,max}} V_{\text{out,max}}}{\omega_0 P_{\text{out}}} = k_D \sqrt{L_{1D} L_{2D}} & (16) \end{cases}$$

$$L_{1D} = \frac{M_D}{k_D} \frac{I_{2D}}{I_{1D}} \sqrt{a}, \quad L_{2D} = \frac{M_D}{k_D} \frac{I_{1D}}{I_{2D}} \frac{1}{\sqrt{a}}. \tag{17}$$

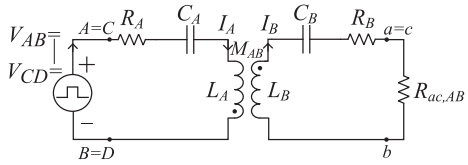

Fig. 5. Equivalent circuit of the conventional one-to-one coil IPT system in the frequency domain. Note that the same semiconductor devices are used as in the V/I-D converter in Fig. 1.

For what concerns the compensation capacitances, their value is selected by imposing $X_i = 0$ in (4) for the secondary coils, i.e., if $i = [3, 4]$. On the other hand, the condition $X_i > 0$ holds for the primary coils, i.e., if $i = [1, 2]$, to ensure slightly inductive primary currents achieving the zero voltage switching (ZVS) turn-ON of all the MOSFETs in Fig. 1 [21], [22], [23].

III. Comparison With One-to-One Coil IPT Systems

To evaluate the advantages of the proposed V/I-D system, its efficiency is compared analytically to the one resulting from a conventional one-to-one coil IPT system with S-S compensation in Fig. 5. A generalized comparison is performed, such that engineers and researchers can evaluate the performance of the proposed system based on their specific application.

A. Circuit Modeling of the One-to-One Coil IPT System

The circuit in the frequency domain of the one-to-one coil IPT system in Fig. 5 is described by the Kirchhoff voltage law in (18). Thereby, the impedance $\boldsymbol{Z_i}$ of the two resonant circuits is defined in (19), and the mutual inductance M_{AB} is expressed in (20), where k_{AB} is the relative coupling factor. $\boldsymbol{V_{AB}}$ is identical to (6). The first-harmonic load $R_{\mathrm{ac},AB}$ depends on the nominal battery voltage, as defined in (21) for the same output power. This one-to-one coil system employs half of the passive components than the V/I-D converter. The same number of MOSFETs and diodes of the V/I-D converter is used to have equal semiconductor costs for the high-frequency inverting and rectifying power conversion stages

$$\begin{cases} \boldsymbol{V_{AB}} = \boldsymbol{Z_A} \boldsymbol{I}_A + j\omega M_{AB} \boldsymbol{I_B} \\ 0 = (\boldsymbol{Z_B} + R_{\mathrm{ac},AB}) \boldsymbol{I_B} + j\omega M_{AB} \boldsymbol{I_A} \end{cases} \tag{18}$$

$$\boldsymbol{Z_i} = R_i + j\omega X_i, \quad X_i = \omega L_i - \frac{1}{\omega C_i}, \quad i = [A, B] \tag{19}$$

$$M_{AB} = k_{AB} \sqrt{L_A L_B} \tag{20}$$

$$R_{\mathrm{ac},AB} = \begin{cases} R_{\mathrm{ac}}, & \text{if tuned for 800-V batteries} \\ R_{\mathrm{ac}}/4, & \text{if tuned for 400-V batteries} \end{cases}. \tag{21}$$

B. Power Conversion Stages

The power conversion stages employed by the V/I-D converter and the one-to-one coil IPT systems are shown in Fig. 6, starting from the grid connection to the EV battery. Both the solutions rely on the regulation of the input voltage since, as explained in [24], the S-S compensation has a current-source output directly proportional to $\boldsymbol{V_{AB}}$. By connecting to the 1-ϕ European 230-V RMS-rated grid line-to-neutral voltage through a boost-like power factor correction (PFC) rectifier, as shown in Fig. 6, V_{in} can be safely regulated in the range of 360–500 V. Lower values of $\boldsymbol{V_{AB}}$ fundamental can be achieved by phase shifting the H-bridge inverters.

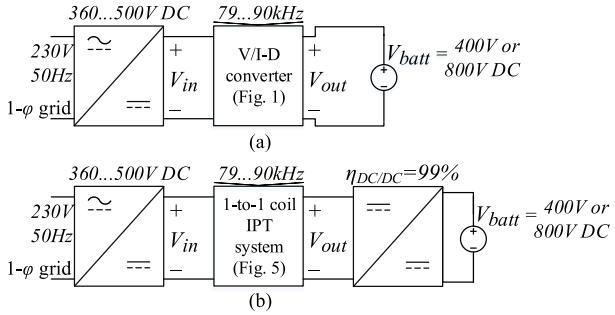

Fig. 6. Power conversion stages of (a) the proposed V/I-D converter and (b) the conventional one-to-one coil IPT system.

TABLE II
Input Parameters and Semiconductor Devices Used in the Comparison of Section III

Input parameters	P_{out}	7.2 kW	Semiconductors*	M1...M8	C2M0040120D
	V_{out}	400 V, 800 V		$R_{\mathrm{ds,on}}$	50 mΩ
	V_{in}	360...500 V (1ϕ)		E_{off}	1 µJ
	f_0	85 kHz		D1...D8	C4D15120D
	k_D	0.15, 0.25, 0.35		V_F	0.8 V
	Q_D	100–400		r	75 mΩ
	M_D	82.63 µH from (16)		*datasheet values @125 °C	

The V/I-D converter employs only the input voltage control and has a direct connection to the EV battery. On the other hand, the one-to-one coil system is provided with a 99% efficient dc–dc converter, as shown in Fig. 6(b), which would conduct only in the case that the current EV battery voltage differs from the nominal to match the optimum load condition.

C. Assumptions

The comparison between the proposed V/I-D converter and the one-to-one coil system has been performed considering the input parameters and semiconductor devices listed in Table II. Both the systems are designed for the nominal operation such that V_{in} is in the range of 500 V. For the one-to-one coil system, two designs have been considered: one with 400 V as the nominal battery voltage, and the other with 800 V. In both the cases, when the battery voltage differs from the nominal value, the one-to-one coil system can supply the same output power through a dc–dc converter, as shown in Fig. 6(b). Moreover, the option of not using the dc–dc converter is also explored for the 400-V one-to-one coil system. In this case, only the input voltage is regulated to deliver the same output power to 800-V batteries.

The one-to-one circuit parameters in Table III have been chosen in terms of the V/I-D's ones assuming that:

1) at the nominal operating conditions, the lumped conduction power losses are equal in the resonant circuits of the one-to-one coil system and the V/I-D system;

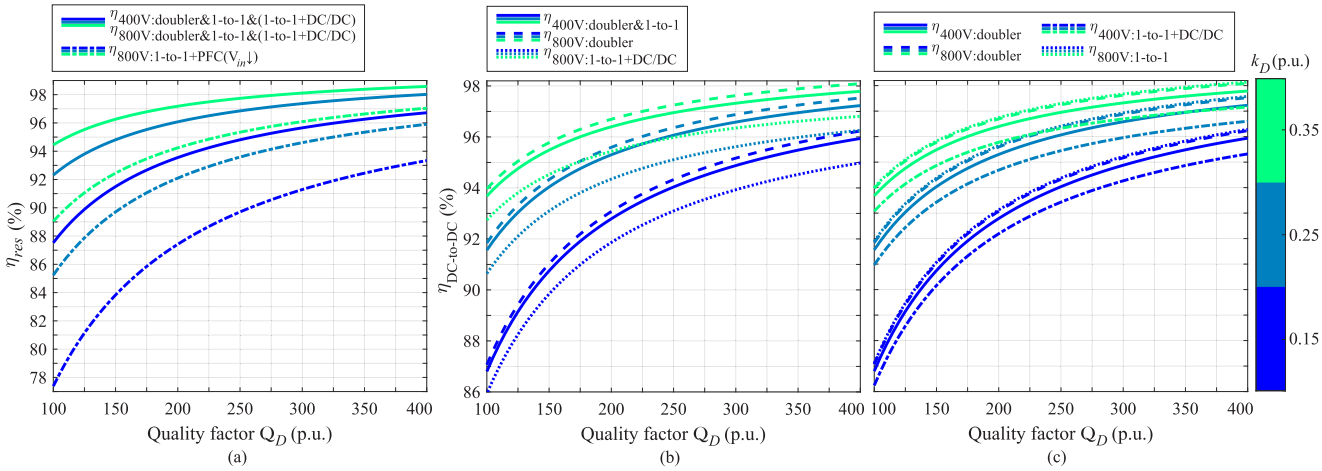

Fig. 7. Analytical power transfer efficiency of the proposed V/I-D converter and the one-to-one coil IPT system at different coils' magnetic coupling k_D and quality factor $Q_D = Q_{1D} = Q_{2D}$ defined in (12). Plot of (a) resonant circuit efficiency and (b) and (c) dc-to-dc efficiency (the power losses consider both the semiconductor devices and resonant circuits), where the one-to-one coil IPT system is designed for a nominal battery voltage of (b) 400 V and (c) 800 V.

TABLE III
CIRCUIT PARAMETERS OF THE CONVENTIONAL 1-TO-1 COIL SYSTEM WITH RESPECT TO THE ONES OF THE PROPOSED V/I-D SYSTEM

	M_{AB}	I_A	L_A	R_A	Q_A
400 V	$M_D/2$	$2 \cdot I_{1D}$	$L_{1D}/2$	$R_{1D}/2$	Q_{1D}
800 V	M_D	$2 \cdot I_{1D}$	$L_{1D}/2$	$R_{1D}/2$	
	k_{AB}	I_B	L_B	R_B	Q_B
400 V	k_D	$2 \cdot I_{2D}$	$L_{2D}/2$	$R_{2D}/2$	Q_{2D}
800 V		I_{2D}	$2 \cdot L_{2D}$	$2 \cdot R_{1D}$	

2) the coefficient a in (15) is considered such that $a = 1$, resulting in the primary and secondary coils having the same quality factor: $Q_{1D} = Q_{2D} = Q_D$.

D. Analysis

The computed efficiency comparison is shown in Fig. 7 in terms of Q_D and k_D. Fig. 7(a) shows the efficiency comparison of the resonant circuits, while Fig. 7(b) and (c) shows the overall dc-to-dc efficiency including the losses of the semiconductor devices whose main parameters are listed in Table II. Thereby, several values of Q_D and k_D are considered for the same M_D in Table II. This makes the analysis generic and applicable to all the typical IPT systems designed at this power level.

Fig. 7(a) shows that, in the two systems, the losses of the resonant circuits stay the same at both 400 and 800 V if the one-to-one coil system uses a dc–dc converter to match the optimum load condition. On the other hand, if the 400-V one-to-one coil system delivers the same power to 800-V batteries by stepping down the input voltage without a dc–dc converter, the power transfer efficiency of the resonant circuit would considerably decrease by up to 10%. This is caused by R_L being four times larger than the nominal optimum condition leading to a higher primary current. Given this large efficiency drop, this solution is discarded in the following comparisons.

Contrarily than in Fig. 7(a), Fig. 7(b) and (c) shows that there is a difference between the computed efficiencies at 400 and 800 V. In the case of solely considering the V/I-D converter, the current doubler mode (400-V battery) has more losses since the number of diode conducting is twice that of the voltage doubler mode (800-V battery). This has been shown in Fig. 2(b). When considering the one-to-one coil system, the designs with 800 V as nominal V_{out} are more efficient than the ones at 400 V since the current flowing through the rectifying diodes is halved for the same power. When comparing the two different systems, the proposed V/I-D system is up to 1% more efficient. For instance, at the same k_D, the two systems would have the same efficiency if the one-to-one coil system is equipped with coils having a larger quality factor. This might put more requirements on the coils' design. For example, when $k_D = 0.35$ in Fig. 7(c), an efficiency of 97% can be reached by the V/I-D converter operating in the current doubler mode (400-V battery) if $Q_D = 250$. The same efficiency can be achieved by the one-to-one coil system when operating with a 400-V battery if the coils have $Q_D = 350$. This difference is even more considerable in Fig. 7(b).

E. Cost and Complexity Considerations

The V/I-D converter has the great advantage of employing only passive semiconductor devices at the secondary circuit, simplifying the circuit and control on board the EV.

Regarding the cost, it is reasonable to assume that the two systems use the same high-frequency inverting and rectifying power conversion stages since each H-bridge of the V/I-D converter is sized for half the power of the one-to-one coil system. When considering the coupled coils, from Table III, it can be deduced that the one-to-one coil system requires using a Litz wire with more strands in the windings, while the core magnetic saturation must also be fulfilled. Thus, the transformer will be naturally sized according to the processed power. Therefore, the size of the components in the two systems would be equivalent if they are fully utilized. Nevertheless, the possible total higher cost of implementing two sets of coupled coils in the V/I-D converter

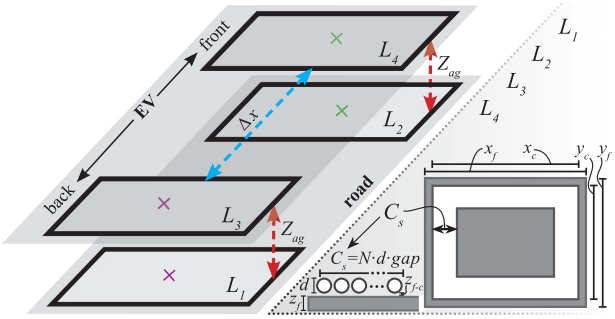

Fig. 8. Coil arrangement of the proposed V/I-D system for EV wireless charging, the circuit schematic of which is shown in Fig. 1.

TABLE IV
MEASURED CIRCUIT PARAMETERS AND COILS' DIMENSIONS

	N	L (μH)	R (mΩ)	M (μH)	Coils' dimensions (mm) with respect to Fig. 8		
L_1	17	246.9	420	M_{13}	x_f, y_f, z_f	C_s	$z_{f\text{-}c}$
L_2	18	276.1	440	80.2	387, 364, 4.1	65	4
L_3	15	185.3	360	M_{24}	x_c, y_c, d	Z_{ag}	Δx
L_4	14	161.7	340	78.5	355, 350, 2.4	100	1000
E planar core: 3C95, PLT43/28/4.1					Litz wire: 600 × 0.071mm		
(C_1, C_2, C_3, C_4) = (14.92, 13.27, 19.05, 21.62)nF →4x(18,16,23,25)* *(series × parallel): KEMET R76TF13305050J 3.3 nF (ESR=0.22 Ω)							

would be undoubtedly overcome by the price of a highly efficient dc–dc converter that must operate in an extensive range, i.e., between 400 and 800 V.

IV. EXPERIMENTAL IMPLEMENTATION

The proposed V/I-D converter has been implemented as a laboratory demonstrator suitable for the 7.7-kW power class.

A. Laboratory Prototype

The two sets of coupled coils have been designed, as shown in Fig. 8. The selection of parameters follows the approach explained in Section II-B, and they are summarized in Table IV. The coils have a different number of turns to prove that the V/I-D converter can also operate in the case that the ideal condition in (12) is not met. The resulting M_{13} and M_{24} are similar, and they are in the same range of the target M_D in Table II. Since the distance Δx between the two sets is much larger than the coils dimensions, their cross-coupling mutual inductances M_{12}, M_{34}, M_{14}, and M_{23} are negligible.

Fig. 9 shows the 7.7-kW prototype, including the compensation capacitors and the power converters. The Delta Elektronika bidirectional power supplies SM500-CP-90 and SM1500-CP-30 are used as input and output voltage sources. The input power supply operates in the voltage range that resembles the boost-like PFC converter, which could be implemented as explained in [25] and [26], while the output power supply emulates the EV battery voltage. It is assumed that V_{in} is set according to the load, the information of which is given by the wireless communication required from the IPT system for several features, such as guided positioning, pairing, and safety.

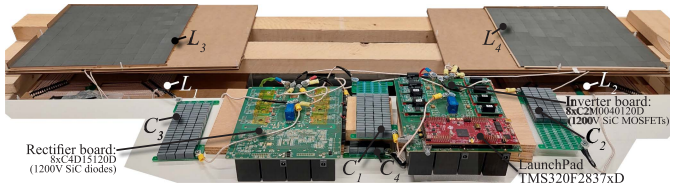

Fig. 9. Developed 7.7-kW V/I-D converter for EV wireless charging.

B. Analysis of the Operating Points

Before validating the functionality of the V/I-D converter experimentally, it is essential to assess the operating points resulting from different misalignment conditions between the coupled coils. In particular, given the sets of coupled coils in Fig. 9, two misalignment profiles have been identified: the lateral misalignment in either the x- or y-direction shown in Fig. 10(a) and the tilted misalignment shown in Fig. 10(b). Considering that the coils are roughly squared shaped, the two directions of lateral misalignment would have a similar impact on the power transfer, and, in that case, M_{13} and M_{24} would vary proportionally. On the other hand, a tilted misalignment would cause an imbalance between M_{13} and M_{24}. The effect of these two misalignment profiles is investigated in Fig. 11 resulting from the analytical model of Section II-A. The performance of the V/I-D converter is assessed in both the voltage doubler (800-V batteries) and current doubler (400-V batteries) modes for an output power of 7.2 kW. The switching frequency of 86.5 kHz is chosen since it is confined within the range of 79–90 kHz established by SAE J2954 [27], and it ensures the ZVS turn-ON of the H-bridge inverters at the nominal alignment with low circulating reactive currents. The performance is assessed in terms of the absolute value and the phase angle of the primary currents $\boldsymbol{I_1}$ and $\boldsymbol{I_2}$, the absolute value of the secondary currents $\boldsymbol{I_3}$ and $\boldsymbol{I_4}$, the $\eta_{\text{DC-to-DC}}$, and the required V_{in}.

Fig. 11(a) addresses the effect of the lateral misalignment on the power transfer. On that purpose, M_{13} and M_{24} are proportionally reduced up to 50% of their nominal value in Table IV. It is possible to notice that the $\eta_{\text{DC-to-DC}}$ drops with the misalignment. This is due to the lower V_{in} required to deliver the same output power, translating into higher primary currents, which worsen the conduction losses. The ZVS turn-ON of the H-bridge inverters is preserved. However, the primary currents become more inductive with the lateral misalignment leading to larger circulating reactive currents and higher turn-OFF losses. The input voltage can be regulated through the PFC rectifier up to 68% of the nominal mutual inductance.

On the other hand, Fig. 11(b) and (c) investigates the effect of the tilted misalignment on the power transfer. Thereby, only one mutual inductance is gradually reduced while keeping the other constant to its nominal value. In the voltage doubler operation, this misalignment profile would eventually cause the hard switching of the H-bridge inverter supplying the coils with higher coupling, while the other H-bridge inverter would operate in a highly inductive region of the resonant circuit. This operation is due to the unbalanced reflected impedance at the primary circuits, while the secondary circuits conduct the same

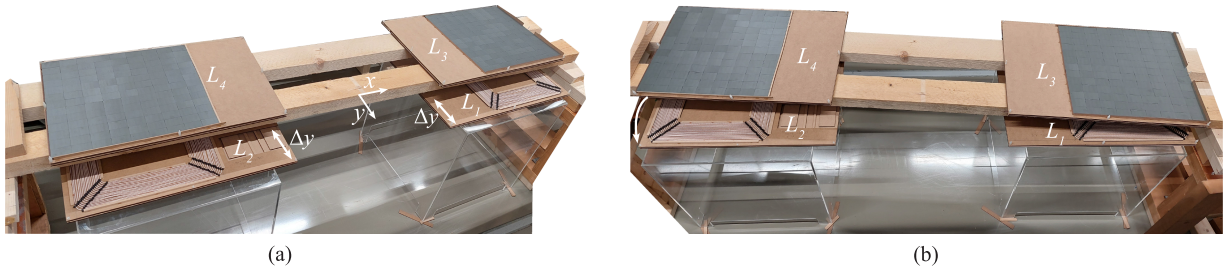

Fig. 10. Coils' position in the presence of (a) lateral misalignment and (b) tilted misalignment.

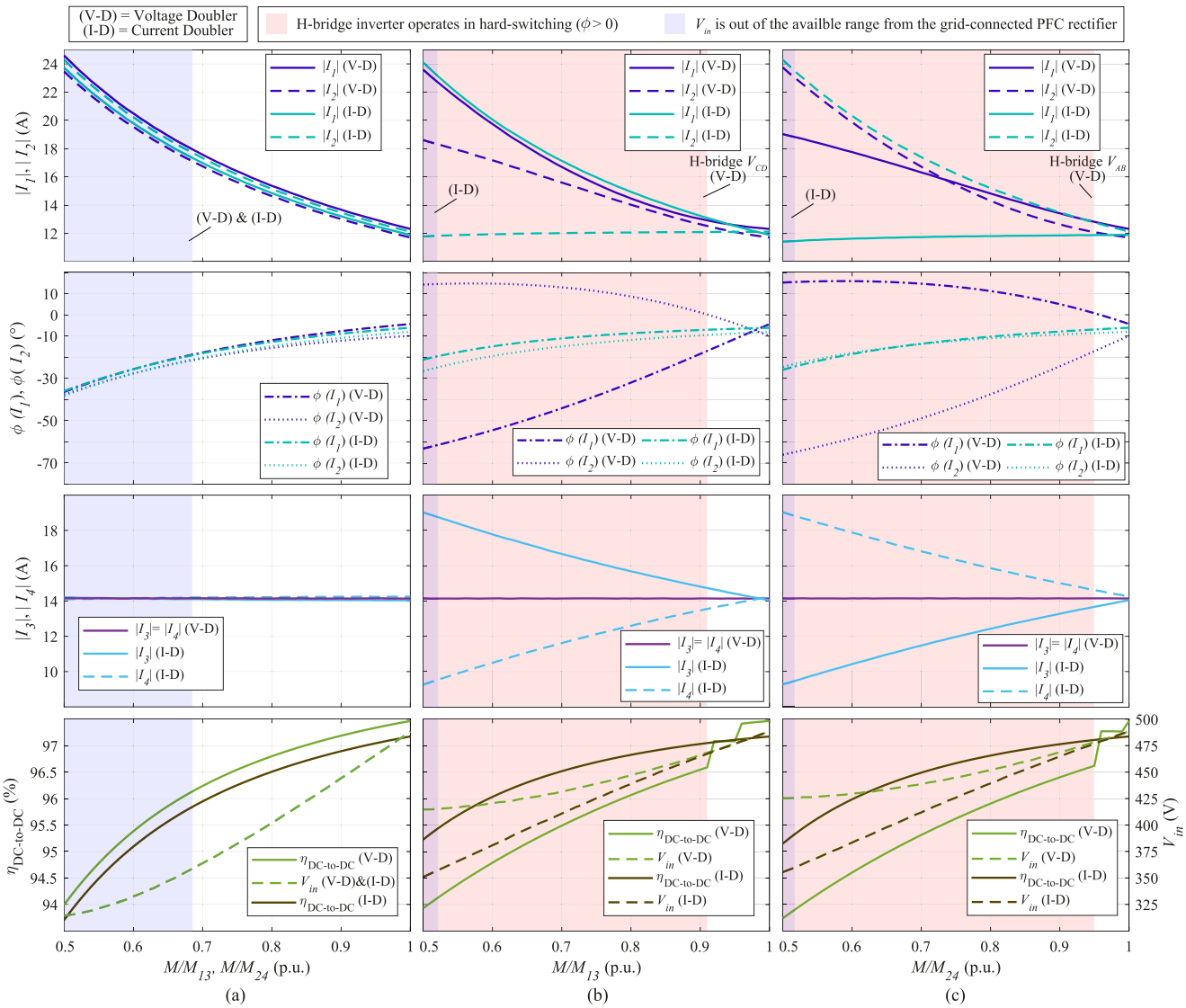

Fig. 11. Operating points of the V/I-D converter in terms of the absolute value and phase angle of $\boldsymbol{I_1}$ and $\boldsymbol{I_2}$, the absolute value of $\boldsymbol{I_3}$ and $\boldsymbol{I_4}$, the $\eta_{\text{DC-to-DC}}$, and the required V_{in} depending on the normalized main mutual inductances with respect to the nominal M_{13} and M_{24} in Table IV. (a) Both M_{13} and M_{24} are varied proportionally (lateral misalignment). (b) Only M_{13} is varied (tilted misalignment). (c) Only M_{24} is varied (tilted misalignment). The results are computed from the analytical model supposing that the output power of 7.2 kW is delivered at a switching frequency of 86.5 kHz. The red-shaded areas denote the operating regions in which the hard switching of the H-bridge inverter occurs. The blue-shaded areas indicate whether the required V_{in} is out of the available range from the grid-connected PFC rectifier.

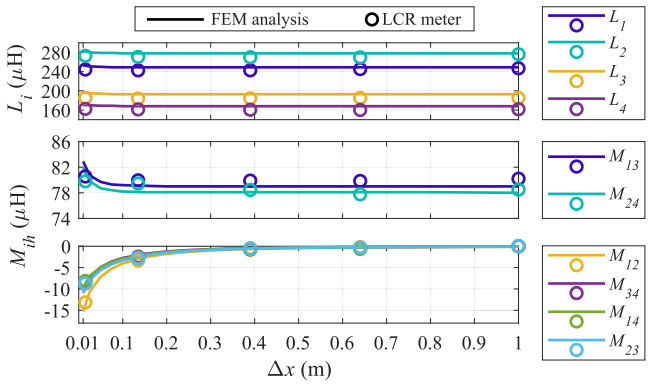

Fig. 12. Values of the self-inductance and the mutual inductance of the four rectangular coils depending on Δx in Fig. 8.

amount of current. This means that the MOSFETs of the inverting stages must be equipped with a suitable thermal management system to withstand the additional power losses introduced by the hard-switching operating points. This behavior is not present in the current doubler operation due to the equivalent parallel connection of the secondary circuits, which allows their currents to be unequal. Nevertheless, the current doubler mode has a considerable current unbalance between the two resonant circuits. In addition, the tilted misalignment requires an input voltage that can be mainly supplied PFC rectifier.

In Fig. 11, the resulting $\eta_{\text{DC-to-DC}}$ is mostly over 94%. Note that the sharp decreases in $\eta_{\text{DC-to-DC}}$ correspond to transitions into hard-switching operating areas.

C. V/I-D Converter's Performance at Lower Values of Δx

In the laboratory demonstrator illustrated in Fig. 9, the two sets of coupled coils are placed considerably far from each other to minimize the undesired cross-coupling. However, in reality, a shorter distance would ease the installation of the proposed V/I-D converter on EVs. For that purpose, it is interesting to assess the minimum distance Δx that would still lead to a negligible cross-coupling.

Fig. 12 shows the values of the self-inductance and the mutual inductance of all four coils depending on Δx resulting from measurement and simulated through the finite-element method (FEM) in COMSOL Multiphysics. The self-inductances, M_{13}, and M_{24} stay approximately constant over Δx. Conversely, the mutual inductances related to the cross-coupling become larger as Δx approaches zero. It must be noted that those instances have negative values due to the direction of the concatenated magnetic field.

To determine the minimum value of Δx that makes the cross-coupling tolerable, the performance of the V/I-D converter has been assessed for the whole range of Δx. This analysis has been performed through the analytical model for an output power of 7.2 kW, a switching frequency of 86.5 kHz, and aligned coils. The results are summarized in Fig. 13. The operating points marked with the light blue-shaded areas, i.e., for $\Delta x > 0.25$ m, would result in a performance similar to the one at $\Delta x = 1$ m used in Fig. 9. Nevertheless, it is preferable to conservatively

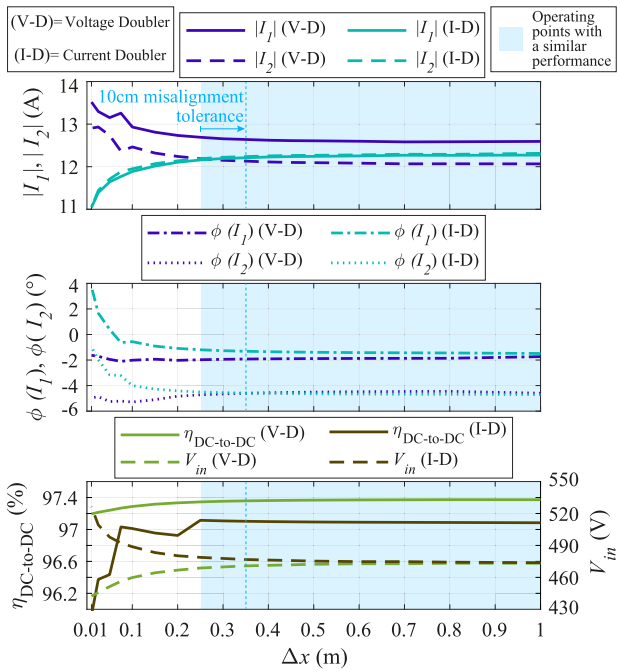

Fig. 13. Analysis of the V/I-D converter in terms of the absolute value and phase angle of $\boldsymbol{I_1}$ and $\boldsymbol{I_2}$, the $\eta_{\text{DC-to-DC}}$, and the required V_{in} depending on distance Δx in Fig. 8. The results are computed from the analytical model supposing that the output power of 7.2 kW is delivered at a switching frequency of 86.5 kHz. The light blue-shaded areas denote the operating regions with similar performance.

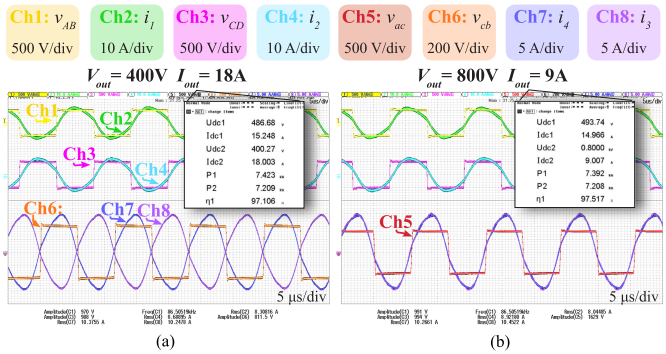

Fig. 14. Measured circuit waveforms and dc-to-dc efficiency with aligned coils when operating at 86.5 kHz and rated power for both nominal V_{out}: (a) current doubler and (b) voltage doubler.

select $\Delta x = 0.35$ m as the minimum distance to guarantee that the cross-coupling would be negligible also when the receiver coils have a lateral misalignment of 10 cm.

V. Experimental Results

The laboratory prototype in Fig. 9 has been tested to prove the functionality of the V/I-D converter.

A. Measurements at the Coils' Nominal Alignment

The circuit waveforms and the dc input and output measurements for the V/I-D system operating at rated power are shown in Fig. 14(a) for the current doubler mode, while Fig. 14(b)

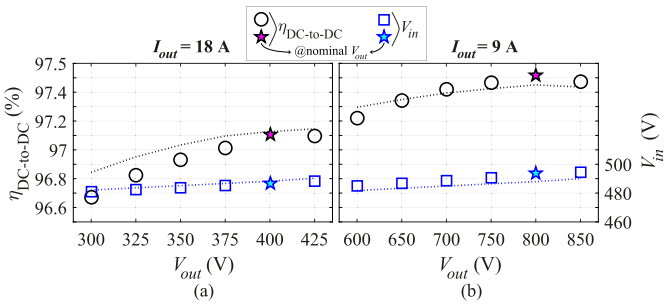

Fig. 15. Measured dc-to-dc efficiency $\eta_{\text{DC-to-DC}}$ and input voltage V_{in} from the prototype in Fig. 9 with aligned coils as (a) current doubler and (b) voltage doubler. The dotted lines result from the analytical model.

TABLE V
MEASURED COILS' PARAMETERS AT THE ALIGNMENTS IN FIG. 10

Fig. 10	L_1 (μH)	L_2 (μH)	L_3 (μH)	L_4 (μH)	M_{13} (μH)	M_{24} (μH)
(a): Δy=7 cm	249.8	278.0	186.2	162.8	69.7	66.3
(a): Δy=9 cm	250.8	279.2	186.5	163.0	57.6	56.6
(b): tilted	247.7	276.7	185.1	162.3	79.7	50.6

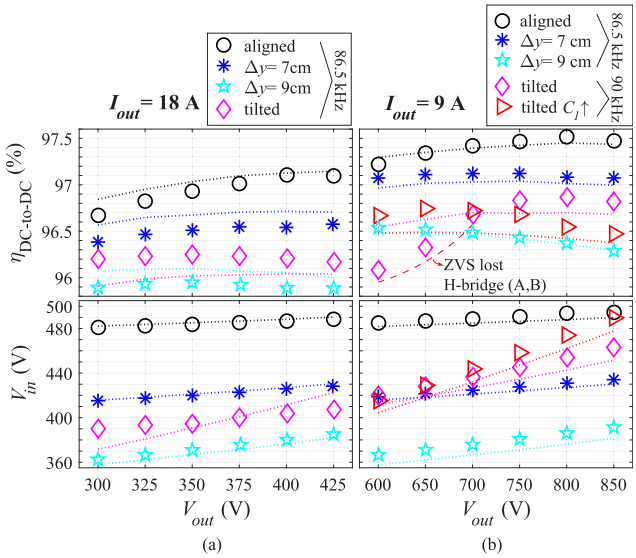

Fig. 16. Measured dc-to-dc efficiency $\eta_{\text{DC-to-DC}}$ and input voltage V_{in} at different coils' alignments as (a) current doubler and (b) voltage doubler. The dotted lines result from the analytical model.

shows the voltage doubler mode. The operation of the H-bridge inverters follows the same logic illustrated in Figs. 2 and 3. The operating frequency of 86.5 kHz selected in Section IV-B leads to the ZVS turn-ON of all MOSFETs. The dc-to-dc efficiency of 97.11% and 97.52% have been measured at 7.2 kW for an output voltage of 400 and 800 V, respectively. As expected, the efficiency is slightly lower in the current doubler mode because the number of diodes conducting is twice that in the voltage doubler mode.

In reality, V_{out} increases during the constant current (CC) mode of the battery charging cycle. Measurements have been performed for (0.75,...,1.06) $\cdot V_{\text{out}}$ while maintaining I_{out} constant. These measurements are summarized in Fig. 15. This also proves that the proposed V/I-D operation works even if V_{out} is not exactly 400 or 800 V, as shown in Table I. During the CV mode of the battery charging cycle, I_{out} should be gradually reduced until the battery is fully charged. According to [28], the S-S compensation can achieve both the CC and CV modes, in which the CV mode can be realized by stepping down V_{in} through the PFC rectifier. Lower values of V_{AB} can be achieved by phase shifting the H-bridge inverters. Hereby, the CV mode is not included since this is not the main focus of this article, and its control strategies are well known from the literature. In addition, for the power level of 7.7 kW, the CC mode takes place for most of the EV battery charging profile. Therefore, it is more critical to ensure high power transfer efficiency during that period to reduce the overall energy consumption.

B. Measurements With Coils' Misalignment

The functionality of the V/I-D converter has been assessed for the misalignment positions shown in Fig. 10; parameters are listed in Table V.

The overall measured $\eta_{\text{DC-to-DC}}$ and the relative V_{in} are shown in Fig. 16. As expected from the analysis of Section IV-B, the dc-to-dc efficiency drops when the misalignment occurs. For the considered coils' alignments, it is possible to follow the entire CC charging using a V_{in} range that the PFC rectifier can provide.

With lateral misalignment at $\Delta y = 9$ cm, the efficiency measured at the nominal V_{out} drops by 1.15% and 1.22% in the voltage doubler and the current doubler modes, respectively. This is due to higher primary currents increasing the conduction losses for the same output power. Since M_{13} and M_{24} decrease proportionally, balanced currents flow through the primary and secondary circuits. In addition, by operating at the same frequency of 86.5 kHz as with the aligned coils, it is possible to keep the ZVS turn-ON for the entire CC charging. These considerations can be noticed in the measured waveforms of Fig. 17(a)–(d).

On the other hand, when considering the tilted misalignment, M_{13} and M_{24} do not decrease proportionally. This translates into unbalanced currents within the primary and secondary circuits in both the current doubler and voltage doubler operations, whose waveforms are shown in Fig. 17(e) and (f), respectively. In the voltage doubler operation, the considerable difference between M_{13} and M_{24} would cause the hard switching of the H-bridge inverter with A and B terminals. To mitigate this issue, the switching frequency of both the inverters has been increased to 90 kHz. Nevertheless, at partial load, the hard switching still occurs, causing the efficiency drop shown in Fig. 16(b), of which the waveforms measured at $V_{\text{out}} = 600$ V are shown in Fig. 17(g). Considering that the operation falls slightly in the capacitive region only at partial load, this extra loss can be considered acceptable, especially in the case that the H-bridge inverters employ SiC MOSFETs with forced cooling.

An alternative solution to achieve the ZVS turn-ON for the entire CC mode during the voltage doubler mode with tilted misalignment is increasing the value of C_1 to make the equivalent impedance $\boldsymbol{Z_1}$ more inductive. According to Fig. 16(b), increasing C_1 from 14.92 to 17.39 nF results in higher measured

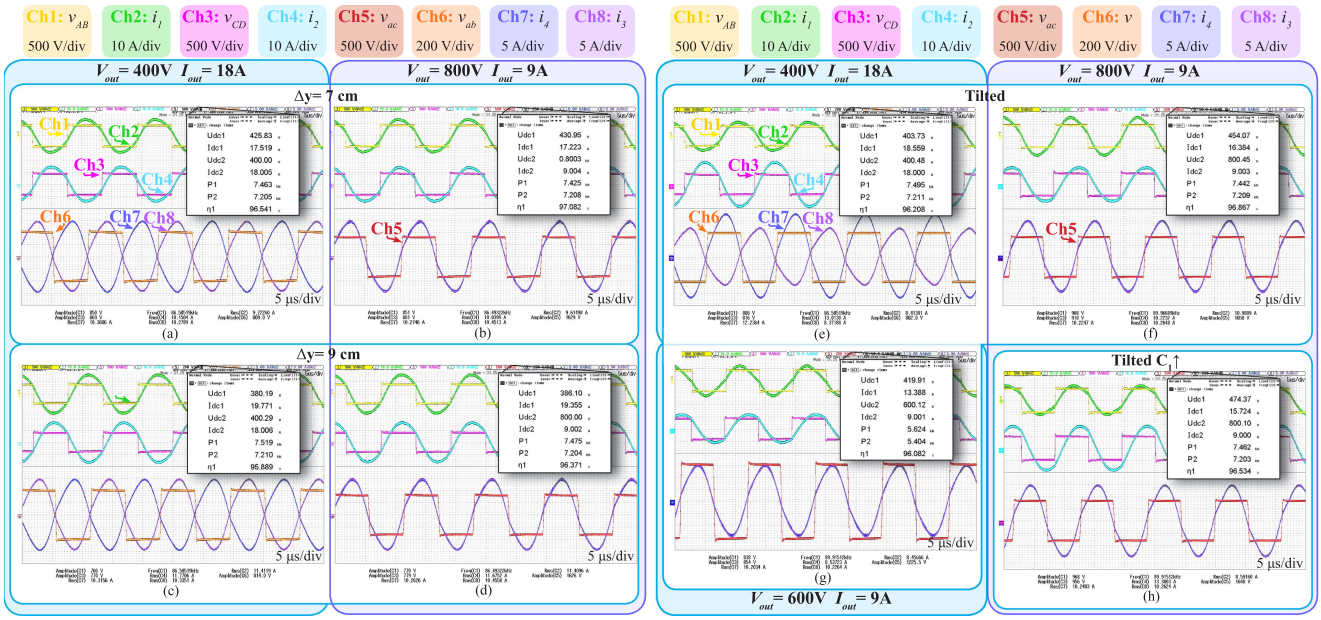

Fig. 17. Measured circuit waveforms and dc-to-dc efficiency in the presence of misalignment. Operation at 86.5 kHz and rated power for both nominal V_{out} with the lateral misalignment [see Fig. 10(a)] when $\Delta y = 7$ cm: (a) current doubler and (b) voltage doubler; when $\Delta y = 9$ cm: (c) current doubler and (d) voltage doubler. Operation with tilted alignment [see Fig. 10(b)]: (e) current doubler (86.5 kHz) and (f) voltage doubler (90 kHz) at rated power. (g) Voltage doubler at minimum load ($V_{\text{out}} = 600$ V, 90 kHz). (h) Voltage doubler at rated power (90 kHz) with $C_1 = 17.39$ nF.

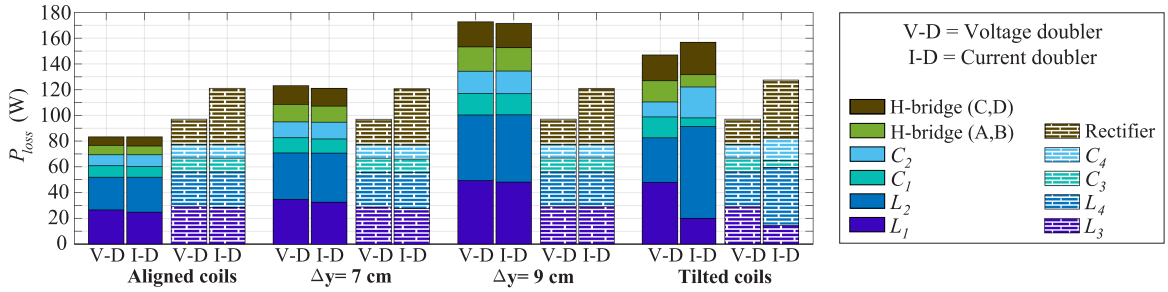

Fig. 18. Breakdown of the computed power losses at both the possible nominal battery voltages at rated power for the different coils' alignments.

$\eta_{\text{DC-to-DC}}$ at partial load. However, $\eta_{\text{DC-to-DC}}$ drops for higher values of V_{out} due to the increase in the amplitude of I_2 visible from Fig. 17(h). Since the capacitance must be set only once before the start of the power transfer, this could be implemented through a mechanical switch.

C. Power Loss Analysis

The power loss breakdown of the V/I-D converter has been computed from the analytical models of Section II for the different coils' alignments, which results in Fig. 18. The efficiency drop in correspondence of the coils' misalignment is due to the higher circulating current in the primary circuits for the same output power. In addition, when the lateral misalignment in Fig. 10(a) occurs, the power losses increase proportionally in both the primary circuits. On the other hand, when the coils have the tilted misalignment shown in Fig. 10(b), it is possible to notice the unbalance in the power losses. For instance, the set of coupled coils with lower mutual inductance would have higher current stress. Nevertheless, the operation of the V/I-D converter would still take place.

VI. Conclusion

This article proposed a new topology defined as V/I-D for EV wireless charging that supplies the same power with high efficiency to both 400- and 800-V batteries. The V/I-D comprises two sets of series-compensated coupled coils connected to a dedicated H-bridge converter. The control was implemented at the primary side by operating the two H-bridge inverters with the same or opposite modulation. The secondary circuit was composed of only passive devices. It was found that the V/I-D system can be more advantageous in terms of computed power transfer efficiency (up to 1%) than the conventional one-to-one coil series-compensated IPT system that uses a 99% efficient dc–dc converter, which is operational when the battery voltage

differs from the nominal. Furthermore, the dc–dc converter adds control complexity onboard the EV. The V/I-D system was also found to be more efficient (up to 10%) than the conventional one-to-one coil series-compensated IPT system employing only input voltage control. After that, the proposed V/I-D converter was experimentally verified at 7.2 kW. Considering that the battery voltage could be either 400 or 800 V, the peak dc-to-dc efficiency of 97.11% and 97.52% was measured, respectively. In addition, by regulating the dc input voltage in the range that a PFC rectifier could provide, the functionality of the V/I-D converter was proved under different misalignments. At 9-cm lateral misalignment, the dc-to-dc efficiency dropped to 95.89% and 96.37% for the output voltage of 400 and 800 V, respectively. Finally, the operation in which the axis connecting the geometrical centers of the secondary coils is tilted with respect to one of the primary coils was also proved. The mutual inductance differs considerably between the two sets of coupled coils, resulting in an uneven distribution of power losses within the primary and secondary circuits. Nevertheless, the functionality of the V/I-D converter was proved to be still valid.

REFERENCES

[1] "Voltage classes for electric mobility," ZVEI—German Electrical and Electronic Manufacturers' Association Centre, 2013. [Online]. Available: https://www.zvei.org/fileadmin/user_upload/Presse_und_Medien/Publikationen/2014/april/Voltage_Classes_for_Electric_Mobility/Voltage_Classes_for_Electric_Mobility.pdf

[2] C. Jung, "Power up with 800-V systems: The benefits of upgrading voltage power for battery-electric passenger vehicles," *IEEE Electrific. Mag.*, vol. 5, no. 1, pp. 53–58, Mar. 2017.

[3] I. Aghabali, J. Bauman, P. J. Kollmeyer, Y. Wang, B. Bilgin, and A. Emadi, "800-V electric vehicle powertrains: Review and analysis of benefits, challenges, and future trends," *IEEE Trans. Transp. Electrific.*, vol. 7, no. 3, pp. 927–948, Sep. 2021.

[4] D.-W. Lee, B.-S. Lee, J.-H. Ahn, J.-Y. Kim, and J.-K. Kim, "New combined OBC and LDC system for electric vehicles with 800 V battery," *IEEE Trans. Ind. Electron.*, vol. 69, no. 10, pp. 9938–9951, Oct. 2022.

[5] R. Bosshard and J. W. Kolar, "All-SiC 9.5 kW/dm3 on-board power electronics for 50 kW/85 kHz automotive IPT system," *IEEE Trans. Emerg. Sel. Topics Power Electron.*, vol. 5, no. 1, pp. 419–431, Mar. 2017.

[6] J. Pries, V. P. N. Galigekere, O. C. Onar, and G.-J. Su, "A 50-kw three-phase wireless power transfer system using bipolar windings and series resonant networks for rotating magnetic fields," *IEEE Trans. Power Electron.*, vol. 35, no. 5, pp. 4500–4517, May 2020.

[7] W. Shi et al., "Design of a highly efficient 20 kW inductive power transfer system with improved misalignment performance," *IEEE Trans. Transp. Electrific.*, vol. 8, no. 2, pp. 2384–2399, Jun. 2022.

[8] EVSpecifications. Accessed: May 10, 2022. [Online]. Available: www.evspecifications.com/

[9] Audi e-tron—Battery and Safety, Audi Technology Portal, Accessed: May 10, 2022. [Online]. Available: www.audi-technology-portal.de/en/

[10] *2018 LEAF First Responders' Guide*, 2018 NISSAN INTERNATIONAL SA, Rolle, Switzerland. Accessed: May 10, 2022. [Online]. Available: www-europe.nissan-cdn.net/content/dam/Nissan/ireland/Brochures/First%20Responders%20Guide/2018%20Leaf%20First%20Responders%20Guide.pdf

[11] *2014 MODEL S Emergency Response Guide*, TESLA MOTORS, INC, Austin, TX, USA. Accessed: May 10, 2022. [Online]. Available: www.tesla.com/sites/default/files/downloads/2014_Model_S_Emergency_Response_Guide_en.pdf

[12] *International Driving Presentation of the New e-Golf*, Volkswagen, Wolfsburg, Germany. Accessed: May 10, 2022. [Online]. Available: www.volkswagen-newsroom.com/en/

[13] *IONIQ 5*, Hyundai Motor U.K. Limited, Leatherhead, U.K. Accessed: May 10, 2022. [Online]. Available: www.hyundai.co.uk/new-cars/ioniq5

[14] *Sophisticated Thermal Management, up to 800-Volt System Voltage*, Dr. Ing. h.c. F. Porsche AG, Stuttgart, Germany. Accessed: May 10, 2022. [Online]. Available: media.porsche.com/mediakit/taycan/en/porsche-taycan/die-batterie

[15] R. Bosshard, J. W. Kolar, and B. Wunsch, "Control method for inductive power transfer with high partial-load efficiency and resonance tracking," in *Proc. Int. Power Electron. Conf.*, 2014, pp. 2167–2174.

[16] S. Bandyopadhyay, P. Venugopal, J. Dong, and P. Bauer, "Comparison of magnetic couplers for IPT-based EV charging using multi-objective optimization," *IEEE Trans. Veh. Technol.*, vol. 68, no. 6, pp. 5416–5429, Jun. 2019.

[17] D. Zhang and D. Zhang, "Flexible-structured phase-shifted multiple-full-bridge dc-dc power supply with wide range output," *IET Power Electron.*, vol. 9, no. 1, pp. 132–141, 2016.

[18] H. Wu, X. Zhan, and Y. Xing, "Interleaved LLC resonant converter with hybrid rectifier and variable-frequency plus phase-shift control for wide output voltage range applications," *IEEE Trans. Power Electron.*, vol. 32, no. 6, pp. 4246–4257, Jun. 2017.

[19] R. L. Steigerwald, "A comparison of half-bridge resonant converter topologies," *IEEE Trans. Power Electron.*, vol. 3, no. 2, pp. 174–182, Apr. 1988.

[20] S. Li and C. C. Mi, "Wireless power transfer for electric vehicle applications," *IEEE Trans. Emerg. Sel. Topics Power Electron.*, vol. 3, no. 1, pp. 4–17, Mar. 2015.

[21] S. Li, W. Li, J. Deng, T. D. Nguyen, and C. C. Mi, "A double-sided LCC compensation network and its tuning method for wireless power transfer," *IEEE Trans. Veh. Technol.*, vol. 64, no. 6, pp. 2261–2273, Jun. 2015.

[22] T. Kan, T. Nguyen, J. C. White, R. K. Malhan, and C. C. Mi, "A new integration method for an electric vehicle wireless charging system using LCC compensation topology: Analysis and design," *IEEE Trans. Power Electron.*, vol. 32, no. 2, pp. 1638–1650, Feb. 2017.

[23] F. Grazian, T. B. Soeiro, P. van Duijsen, and P. Bauer, "Auto-resonant detection method for optimized ZVS operation in IPT systems with wide variation of magnetic coupling and load," *IEEE Open J. Ind. Electron. Soc.*, vol. 2, pp. 326–341, 2021.

[24] W. Zhang and C. C. Mi, "Compensation topologies of high-power wireless power transfer systems," *IEEE Trans. Veh. Technol.*, vol. 65, no. 6, pp. 4768–4778, Jun. 2016.

[25] J. W. Kolar, J. Biela, and J. Minibock, "Exploring the Pareto front of multi-objective single-phase PFC rectifier design optimization—99.2% efficiency vs. 7kW/din^3 power density," in *Proc. IEEE 6th Int. Power Electron. Motion Control Conf.*, 2009, pp. 1–21.

[26] J. P. M. Figueiredo, F. L. Tofoli, and B. L. A. Silva, "A review of single-phase PFC topologies based on the boost converter," in *Proc. 9th IEEE/IAS Int. Conf. Ind. Appl.*, 2010, pp. 1–6.

[27] *J2954 (R) Wireless Power Transfer for Light-Duty Plug-In/Electric Vehicles and Alignment Methodology*, SAE Int. Standard, Oct. 2020.

[28] H. T. Nguyen et al., "Review map of comparative designs for wireless high-power transfer systems in EV applications: Maximum efficiency, ZPA, and CC/CV modes at fixed resonance frequency independent from coupling coefficient," *IEEE Trans. Power Electron.*, vol. 37, no. 4, pp. 4857–4876, Apr. 2022.

Francesca Grazian (Student Member, IEEE) received the bachelor's degree in electrical engineering from the University of Bologna, Bologna, Italy, in 2016, and the master's degree in electrical engineering in 2018 from the Delft University of Technology, Delft, The Netherlands, where she is currently working toward the Ph.D. degree.

Her research interests include power electronics and wireless power transfer for battery charging.

Miss Grazian was the recipient of the Best Poster Award in the 2022 European PhD School organized by the European Center for Power Electronics (ECPE) and Best Paper award in the 2022 International Conference on Power Electronics and Motion Control.

Thiago Batista Soeiro (Senior Member, IEEE) received the B.Sc. (Hons.) and M.Sc. degrees in electrical engineering from the Federal University of Santa Catarina, Florianopolis, Brazil, in 2004 and 2007, respectively, and the Ph.D. degree in high efficiency electrostatic precipitator systems with low effects on the mains from the Swiss Federal Institute of Technology, Zurich, Switzerland, in 2012.

During his master's and Ph.D. studies, he was a Visiting Scholar with the Power Electronics and Energy Research Group, Concordia University, Montreal, QC, Canada, and with the Center for Power Electronics Systems, Virginia Tech, Blacksburg, VA, USA. From 2012 to 2013, he was a Researcher with the Power Electronics Institute, Federal University of Santa Catarina. From October 2013 to April 2018, he was with the Corporate Research Center, ABB Switzerland Ltd., Baden-Dattwil, Switzerland, where he was a Senior Scientist. From May 2018 to January 2022, he was with the DC Systems, Energy Conversion, and Storage Group, Delft University of Technology, Delft, The Netherlands, where he was an Associate Professor. Since 2022, he has been with the Power Management and Distribution Section, European Space Research and Technology Centre, European Space Agency, Noordwijk, The Netherlands. In October 2022, he will join the Power Electronics and Electromagnetic Compatibility Group, University of Twente, Enschede, The Netherlands, as a Full Professor. His research interests include advanced high-power converters and dc system integration.

Dr. Soeiro was a recipient of the 2013 IEEE Industrial Electronics Society Best Conference Paper Award and the Best Paper Awards in the following IEEE conferences: International Conference on Power Electronics—ECCE Asia 2011, the 2013 International Conference on Industrial Technology, the Conference on Power Electronics and Applications—ECCE Europe 2015, and 2020 International Conference on Power Electronics and Motion Control.

Pavol Bauer (Senior Member, IEEE) received the master's degree in electrical engineering from the Technical University of Kosice, Kosice, Slovakia, in 1985, and the Ph.D. degree in dynamic analysis of three-phase AC converters from the Delft University of Technology, Delft, The Netherlands, in 1995.

From 2002 to 2003, he was with KEMA (DNV GL), Arnhem, The Netherlands, where he worked on different projects related to power electronics applications in power systems. He is currently a Full Professor with the Department of Electrical Sustainable Energy, Delft University of Technology, where he is also the Head of DC Systems, Energy Conversion, and Storage Group. He is also a Professor with the Brno University of Technology, Brno, Czech Republic, and an Honorary Professor with the Politehnica University Timişoara, Timişoara, Romania. He has authored or coauthored more than 120 journal articles and 500 conference papers in his field. He is an author or co-author of eight books, holds seven international patents, and organized several tutorials at international conferences. He has worked on many projects for the industry concerning wind and wave energy, power electronic applications for power systems such as Smarttrafo, HVDC systems, and projects for smart cities such as photovoltaic (PV) charging of electric vehicles, PV and storage integration, and contactless charging. He participated in several Leonardo da Vinci and H2020, and Electric Mobility Europe EU projects as a Project Partner (ELINA, INETELE, E-Pragmatic, Micact, Trolley 2.0, OSCD, P2P, and Progressus) and a Coordinator (PEMCWebLab.com-Edipe, SustEner, Eranet DCMICRO).

Dr. Bauer is the Former Chairman of the Benelux IEEE Joint Industry Applications Society and the Power Electronics and Power Engineering Society Chapter, the Chairman of the Power Electronics and Motion Control Council, a Member of the Executive Committee of European Power Electronics Association, and a Member of the International Steering Committee at numerous conferences.